Non-Gaussian Carrier-Derived Doppler Integrity FDE for Multiple GNSS Satellites

Wenying Lei(✉), Hong Han, Wenshan Liu, Fei Ling, and Yansong Meng

China Academy of Space Technology (Xi'an), Xi'an 710100, China
lordleid@163.com

Abstract. In this paper, a real-time multi-satellite non-Gaussian carrier-derived Doppler integrity fault detection and elimination (FDE) method is proposed for the abnormal jump of user clock drift estimation caused by satellite switching for low-earth orbit (LEO) global navigation satellite system (GNSS) users. The carrier-derived Doppler integrity faults of multiple GNSS satellites under non-Gaussian distribution are detected and eliminated by using the nearest neighbor principle of user clock drift constraint. Multiple carrier-derived Doppler faults caused by multiple satellite handoffs can be eliminated and the corresponding abnormal jumps in the user clock drifts are removed. Estimation accuracy and integrity of user clock drift are improved for LEO GNSS clock discipline. The analysis of the measured data shows that the stability of the user clock drift with broadcast ephemeris is improved to 5E-13-2E-12 except that the stability of the user clock with 64-10,000 s is not worse than 5E-13 before 64 s. The abnormal jumps in the user clock drift series estimated with non-Gaussian carrier-derived Doppler can be effectively suppressed for multiple GNSS satellites.

Keywords: RAIM · Non-Gaussian · Carrier-derived Doppler · FDE · User clock drift

1 Introduction

In recent years, with the development of LEO GNSS navigation enhanced satellite system, clock taming technology based on carrier-derived Doppler has great advantages and potential in the establishment and maintenance of frequency reference of LEO satellite. The long-term and short-term stability performance of high-stability crystal oscillator after taming can be comparable to that of satellite-borne atomic clock, and it has an important response. Use value and market competitiveness [1]. The whole clock taming process requires high completeness of carrier Doppler, but the switching factor of satellite can cause millimeter-scale jitter of carrier-derived Doppler measurements, which poses a serious challenge to the integrity of carrier-derived Doppler measurements. Because the error characteristics of carrier phase measurements are non-Gauss distribution, and the error characteristics of carrier-derived Doppler after difference are non-Gauss distribution, the traditional Receiver Autonomous Integrity Monitoring (RAIM) method based on chi-square distribution is not suitable for [2–5].

J. Sun et al. (Eds.): CSNC 2020, LNEE 651, pp. 589–597, 2020.
https://doi.org/10.1007/978-981-15-3711-0_52

At present, there is no good solution to monitor the integrity of carrier-derived Doppler jump caused by satellite handover.

In view of the above problems in carrier-derived Doppler high integrity monitoring, some scholars in the world have done some theoretical research on carrier phase RAIM algorithm. Its representative is the carrier phase RAIM method based on Gauss Mixture Model (Gauss Sum Filter) of Yun, Korea [6]. In order to solve the problem of non-Gaussian distribution of carrier phase, this method uses the distribution of multi-Gaussian distribution to approximate the non-Gaussian error distribution of carrier phase, and gives the method of carrier phase integrity monitoring under Bayesian framework. This method has high computational complexity and is only suitable for post-processing. It has little significance in guiding real-time application theory in engineering practice. In addition, this method is not applicable to the integrity monitoring of carrier Doppler, and cannot solve the integrity monitoring problem of carrier-derived Doppler jump caused by satellite handover.

This paper presents a real-time Fault Detection and Elimination (FDE) method for multi-satellite non-Gaussian carrier-derived Doppler integrity fault detection and removal. The carrier-derived Doppler difference caused by multi-satellite handover can be realized. The detection and elimination of constant jumps overcome the abnormal jump problem of user clock speed sequence introduced by multi-satellite switching, and improve the estimation accuracy and integrity of user clock speed when GNSS is used to tame low orbit satellite clock. It has broad application prospects.

2 Non-Gaussian Carrier-Derived Doppler Measurement Model

The input of autonomous integrity monitoring of carrier-derived Doppler receiver is the carrier-derived Doppler of intermediate epoch which is calculated by the difference of carrier phase between the first and last two epochs in three epochs. In epoch n, The carrier phase of the LEO satellite GNSS receiver for the frequency point f and the GNSS satellite s can be expressed as [7–9]

$$\varphi_{f,r}^{s}(n) = \rho_{r}^{s}(n) + cdt_{r}(n) - cdT^{s}(n) + I_{f,r}^{s}(n) + \lambda_{f}N_{f,r}^{s}(n) + \varepsilon_{\varphi,f}(n) \tag{1}$$

where ρ_{r}^{s} the geometric distance between the phase centers of satellite antenna and receiver antenna, c is the speed of light, dT^{s} and dt_{r} are the clock biases of the satellite clock and receiver clock respectively, $I_{f,r}^{s}$ is the ionospheric error, λ_{f} and $N_{f,r}^{s}$ the wavelength and ambiguity without ionosphere, respectively, represent the carrier phase measurement noise.

Assuming that the satellite s at epoch $n-1$, n, $n+1$ can be simultaneously viewed by the receiver, the carrier-derived Doppler calculation method can be written as follows.

$$D_{f,r}^{s}(n) = -\frac{\left[\varphi_{f,r}^{s}(n+1) - \varphi_{f,r}^{s}(n-1)\right]}{2T_s} \tag{2}$$

where T_s represents the sampling interval between two adjacent epochs. Because the errors of $\varphi_{f,r}^{s}(n+1)$ and $\varphi_{f,r}^{s}(n-1)$ are non-Gaussian distribution, the error of $D_{f,r}^{s}(n)$ is also non-Gaussian distribution. Thus, the pseudorange RAIM algorithm cannot be applied to the receiver autonomous integrity monitoring of carrier derived Doppler.

3 Nearest Neighbor Clock Drift Constrained Carrier-Derived Doppler Integrity FDE

Conventional receiver RAIM method assumes that only one satellite has integrity failure at the same time [7, 10, 11]. However, in the process of carrier-derived Doppler integrity monitoring, it is found that the above processing strategy is not ideal, because there may be two satellites switching simultaneously in the same epoch. The proposed method for detecting and eliminating carrier-derived Doppler integrity anomalies can simultaneously detect and eliminate carrier-derived Doppler anomalies of multiple satellites. In the nth epoch, the hypotheses of carrier-derived Doppler integrity H0 and H1 can be described as:

H0: No integrity abnormality was found in the measured values of carrier-derived Doppler of m satellites with the nth epoch.
H1: The integrity anomaly of carrier-derived Doppler measurements from one to more satellites in m satellites of the nth epoch.

When more than four satellites can be observed at the same time, the unknown vector $\boldsymbol{x} = \left[\boldsymbol{v}_r(n)^T, c\dot{dt}_r(n)\right]^T$ which is composed by the user three-dimensional velocity $\boldsymbol{v}_r(n)$ and user clock drift $\dot{dt}_r(n)$, can be obtained by solving the following formula (3) iteratively.

$$\boldsymbol{b} = \boldsymbol{H}\boldsymbol{x} + \boldsymbol{\varepsilon}_v \tag{3}$$

$$\boldsymbol{b} = \begin{bmatrix} D_{f,r}^{1}(n) - \boldsymbol{v}^{1}(n)^T \boldsymbol{e}_r^{1}(n) - \dot{d}_{r,Sag}^{1}(n) + cd\dot{T}^{1} \\ D_{f,r}^{2}(n) - \boldsymbol{v}^{2}(n)^T \boldsymbol{e}_r^{2}(n) - \dot{d}_{r,Sag}^{2}(n) + cd\dot{T}^{2} \\ \vdots \\ D_{f,r}^{m}(n) - \boldsymbol{v}^{m}(n)^T \boldsymbol{e}_r^{m}(n) - \dot{d}_{r,Sag}^{m}(n) + cd\dot{T}^{m} \end{bmatrix} \tag{4}$$

$$\boldsymbol{H} = \begin{bmatrix} -\boldsymbol{e}_r^{1}(n)^T & 1 \\ -\boldsymbol{e}_r^{2}(n)^T & 1 \\ \vdots & \vdots \\ -\boldsymbol{e}_r^{m}(n)^T & 1 \end{bmatrix} \tag{5}$$

where $\boldsymbol{v}^s(n) = \left[v_x^s(n), v_y^s(n), v_z^s(n)\right]^T, s = 1, 2, \ldots, m$ denotes the three-dimensional velocities of the observed m GNSS satellites at epoch n. The satellite-to-ground unit vector corresponding to the satellite s can be expressed as

$$\boldsymbol{e}_r^s(n) = [\boldsymbol{r}^s(n) - \boldsymbol{r}_r(n)]/\|\boldsymbol{r}^s(n) - \boldsymbol{r}_r(n)\|_2 \tag{6}$$

where $\boldsymbol{r}^s(n) = [x^s(n), y^s(n), z^s(n)]^T$ represents the three-dimensional position of the corresponding GNSS satellite. $\boldsymbol{r}_r(n) = [x_r(n), y_r(n), z_r(n)]^T$ is the unknown user position。Sagnac changing rate $\dot{d}_{r,Sag}^s(n)$ can be expressed as

$$\dot{d}_{r,Sag}^s(n) = \frac{\omega_e}{c}\begin{bmatrix} v_y^s(n)x_r(n) + y^s(n)v_{x,r}(n) - \\ v_x^s(n)y_r(n) - v_{y,r}(n)x^s(n) \end{bmatrix} \tag{7}$$

where ω_e is the earth rotation rate, $v_{x,r}(n)$ and $v_{y,r}(n)$ are the x and y components in the user three dimensional velocity $\boldsymbol{v}_r(n)$.

After the iteration process solving the unknown vector $\boldsymbol{x}$ stopped, the converged vector can be denoted as $\boldsymbol{x}_0$. The QR orthogonal-triangular decomposition of the corresponding matrix $\boldsymbol{H}$ can be represented as [1–4]

$$\boldsymbol{H} = \boldsymbol{QR} \tag{8}$$

where $\boldsymbol{R}$ is an upper triangular matrix, $\boldsymbol{Q}$ is an orthogonal matrix. Since $\boldsymbol{Q}^{-1} = \boldsymbol{Q}^{\mathrm{T}}$, $\boldsymbol{Q}^{\mathrm{T}}$ can be divided with the following formula

$$\boldsymbol{Q}^{\mathrm{T}} = \begin{bmatrix} \boldsymbol{M}_{(1:4,:)} \\ \boldsymbol{N}_{(5:m,:)} \end{bmatrix} \tag{9}$$

By left multiplying the residual vector $\boldsymbol{b}$ by $\boldsymbol{N}$, we get $\boldsymbol{p} = \boldsymbol{Nb}$. Then the standard deviation of $\boldsymbol{p}$ can be calculated in real-time as $\sigma_d = \boldsymbol{p}^T\boldsymbol{p}/(m-4)$. The vector test statistic $\boldsymbol{T}$ and its corresponding detection threshold with the Gaussian distribution approximation are denoted as

$$\boldsymbol{T} = \boldsymbol{p}^T\boldsymbol{N}./(\sigma_d\sqrt{sum(\boldsymbol{N}. \times \boldsymbol{N}, 1)}) \tag{10}$$

$$Thd = \mu \cdot std(\boldsymbol{T}),\ \mu \in \{1, 2, 3\} \tag{11}$$

where $.\times$ represents element-wise multiplication. $sum(\boldsymbol{A}, 1)$ operates on successive elements in the columns of A and returns a row vector of the sums of each column, μ is the threshold multiplier. The carrier-derived Doppler anomalies can be detected by comparing the vector test statistic **T** with its Thd. The decision rules are: if $\boldsymbol{T} > Thd$, the hypothesis H1 is accepted; if $\boldsymbol{T} \leq Thd$, then the hypothesis H0 is accepted. When the hypothesis H1 is accepted, collect the satellite numbers into the set Ω which meet the condition $\boldsymbol{T} > Thd$. The number of elements in Ω is denoted as df.

The visible satellite number at epoch n is denoted as Υ. Exterminating all possible combinations of the elements of df taken $1 \sim df$ at a time from Ω using $C_{df}^{1}, C_{df}^{2}, \ldots, C_{df}^{df}$, then a series of the candidate sets can be expressed as $\Omega_1, \Omega_2, \ldots, \Omega_{df}$, The candidate user velocities and clock drifts can be listed in the following sets as

$$\mathrm{X}_1 = \{\boldsymbol{x}_1^S\}, \;\; S \in \Upsilon \backslash q, \; q \in \Omega_1, card(\mathrm{X}_1) = \frac{df!}{(df-1)!} \tag{12}$$

$$\mathrm{X}_2 = \{\boldsymbol{x}_2^S\}, \;\; S \in \Upsilon \backslash q, \; q \in \Omega_2, card(\mathrm{X}_2) = \frac{df!}{2(df-2)!} \tag{13}$$

$$\cdots\cdots$$

$$\mathrm{X}_{df} = \{\boldsymbol{x}_{df}^S\}, \;\; S \in \Upsilon \backslash q, \; q \in \Omega_{df}, card(\mathrm{X}_{df}) = 1 \tag{14}$$

in which $card(\cdot)$ is the number of elements in a set. The optimal user velocity and clock drift can be chosen from the following union set

$$\mathrm{X}_{ensemble} = \mathrm{X}_1 \cup \mathrm{X}_2 \cup \ldots \cup \mathrm{X}_{df} \cup \{\mathbf{x}_0\} \tag{15}$$

The optimal user velocities and clock drift is denoted as $\boldsymbol{x}^*(n) = \left[\boldsymbol{v}_r^*(n)^T, cd\dot{t}_r^*(n)\right]^T$, the initial value is $\boldsymbol{x}^*(0) = \boldsymbol{x}_0$. The average user clock drift can be recursively calculated as

$$\overline{cd\dot{t}_r^*}(n-1) = \frac{n-2}{n-1}\overline{cd\dot{t}_r^*}(n-2) + \frac{cd\dot{t}_r^*(n-1)}{n-1} \tag{16}$$

The rule of minimum absolute error is adopted to find the optimal index of the optimal $\boldsymbol{x}^*(n)$ in $\mathrm{X}_{ensemble}$

$$i = \underset{i}{\operatorname{argmin}}\left\{\left|\mathrm{X}_{ensemble}\{i\}_4 - \overline{cd\dot{t}_r^*}(n-1)\right|\right\} \tag{17}$$

$$\boldsymbol{x}^*(n) = \mathrm{X}_{ensemble}\{i\} \tag{18}$$

where $\mathrm{X}_{ensemble}\{i\}_4$ represents the 4th component in the ith element of $\mathrm{X}_{ensemble}$. Through the above approach, multiple non-Gaussian carrier-derived Doppler faults can be effectively detected and eliminated.

4 Experiment Results

This section receives GPS RF signal data generated by Spirent simulator through Trimble Net R9 receiver, and uses hydrogen clock to provide 10 MHz reference frequency signal of the same source for Spirent simulator and Trimble receiver. Since the LEO receiver uses a dual-frequency ionospheric-free combination to eliminate 99.9%

of the ionospheric delay error, Spirent turns off the ionospheric and tropospheric delays when simulating GPS signals. Without using carrier-derived Doppler abnormal jumping and eliminating methods, the user clock speed calculated by carrier-derived Doppler in observation period and the variation rule of visible satellite are shown in Fig. 1.

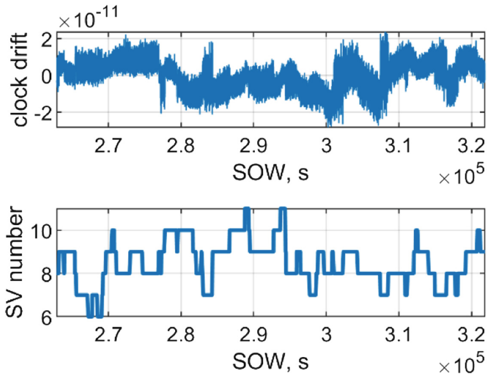

Fig. 1. User clock drift against visible satellite number variation without carrier-derived Doppler integrity FDE

The standard deviation of user clock speed in Fig. 1 is 2.3 mm. As can be seen from Fig. 1, the fluctuation of user clock speed without carrier-derived Doppler FDE is obvious, and the accuracy and stability of the user clock after taming will be directly reduced by using such clock speed estimation. In theory, since the frequency of Trimble receiver and Spirent simulator is homologous to the hydrogen clock, the clock speed of the receiver should theoretically be stable near zero. In addition, the number of satellites is switched frequently during the whole observation process, and the switching of satellites corresponds to the jump of user clock speed estimation. Therefore, it can be determined that one of the factors leading to the change of satellite clock speed is due to satellite switching.

According to the traditional RAIM algorithm assumption, only one satellite's carrier-derived Doppler observations occur RAIM fault at a time. First, in Formula (11), the list of satellites exceeding the threshold is detected and counted. The satellite whose absolute value exceeds the threshold is selected and the result is shown in Fig. 2.

The standard deviation of the user's clock speed in Fig. 2 is 3.1 mm. From Fig. 2, after the detection and removal of a faulty satellite, the estimation curve of user clock speed is generally flatter, but in some areas, the user clock speed is worse than that without FDE, which exceeds 6E-11, so the clock speed estimation jumps greatly. The reason is that satellite switching may exceed one at a time, and the measurement value of only one satellite cannot eliminate the clock rate jump caused by multiple switching, which can be confirmed by the satellite change curve in Fig. 1. The curve of user clock speed estimation is shown in Fig. 3 after detecting and eliminating multiple fault satellites by the method presented in this paper.

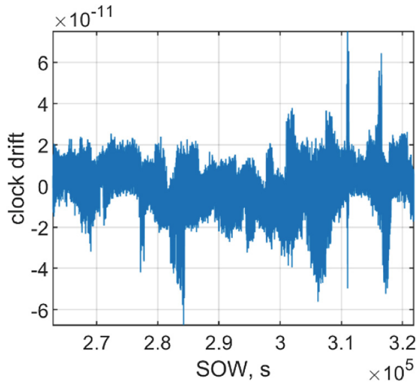

Fig. 2. User clock drift after removing 1 faulted satellite

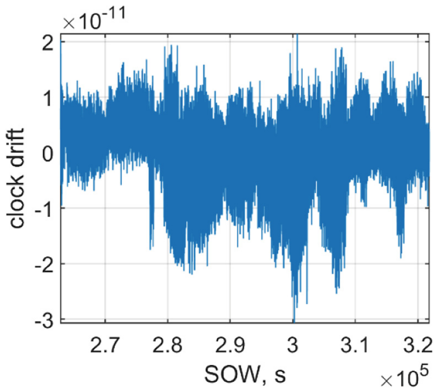

Fig. 3. User clock drift after removing multiple faulted satellites

The standard deviation of user clock speed in Fig. 3 is 1.6 mm. From Fig. 3, it can be seen that the accuracy of the user clock speed after the detection and removal of multiple faulty satellites by this method is significantly higher than that of the user clock speed of the non-carrier-derived Doppler integrity FDE and that of the user clock speed of only one faulty satellite detected and removed, and the change of the user clock speed is more stable in the whole observation interval. In Fig. 4, a comparison of the effects of carrier-derived Doppler integrity FDE of multiple satellites on improving user clock stability is given.

As can be seen from Fig. 4, the stability of the multi-satellite carrier-derived Doppler integrity FDE method in this paper deteriorated slightly before 64 s, and the deterioration range was less than 5E-13. After 64 s, the medium-term and long-term stability of the multi-satellite carrier-derived Doppler integrity FDE method improved significantly, and the improvement range was 5E-13 ~ 2E-12. The slight deterioration of stability before 64S is due to the use of the information of the average user clock difference at the front L-point in the carrier-derived Doppler RAIM algorithm proposed in this paper.

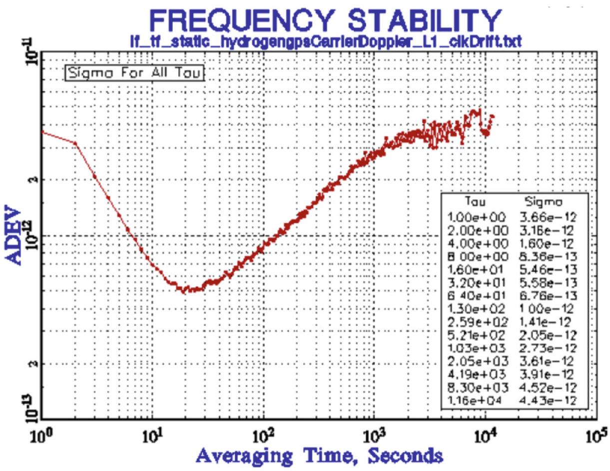

(a)

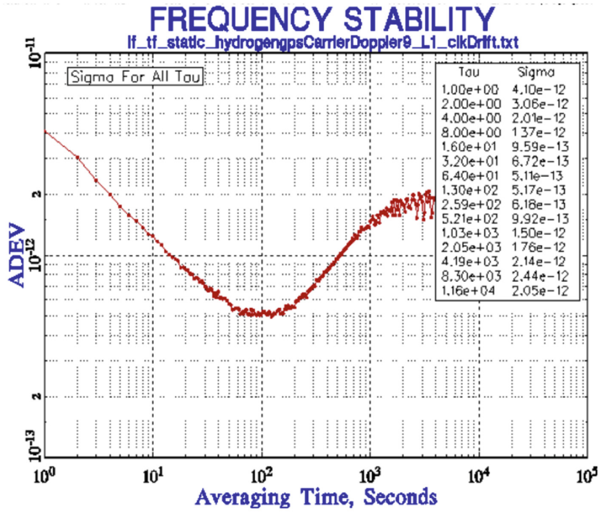

(b)

Fig. 4. Comparison of user clock stability performance before and after multiple satellite carrier-derived Doppler FDE. (a) user frequency stability without FDE; (b) user frequency stability with multiple fault satellite FDE

5 Conclusions

In this paper, a multi-satellite non-Gaussian carrier-derived Doppler integrity fault detection and elimination method is studied. The nearest neighbor clock speed constraint model can detect and eliminate the carrier-derived Doppler anomaly of multiple satellites under non-Gaussian distribution. It can effectively suppress the user clock jitter caused by simultaneous switching of multiple satellites and improve the medium and long-term stability of user clock speed estimation. The experimental results show that the stability of users using broadcast ephemeris is improved from 64 s to 10,000 s, except that the stability before 64 s is not worse than 5E-13. The research results in this paper can realize the autonomous monitoring of carrier-derived Doppler integrity of multi-satellite non-Gaussian distribution, satisfy the application requirements of integrity monitoring of carrier-derived Doppler observations of LEO satellites, and satisfy the requirements of real-time processing on LEO satellites. It can provide real-time and high-precision estimation of clock speeds of LEO satellites using carrier-derived Doppler in the future. Domestication provides a theoretical basis.

Acknowledgment. This work is supported by National Natural Science Foundation of China (61627817, 11803023).

References

1. Joerger, M., et al.: Analysis of iridium-augmented GPS for floating carrier phase positioning. Navigation **57**(2), 137–160 (2010)
2. Feng, S., Ochieng, W., Moore, T., et al.: Carrier phase-based integrity monitoring for high-accuracy positioning. GPS Solut. **13**(1), 13–22 (2009)
3. Osechas, O., Misra, P., Rife, J.: Carrier-phase acceleration RAIM for GNSS satellite clock fault detection. Navigation **59**(3), 221–235 (2012)
4. Zhang, Q., Gui, Q.: Carrier-phase RAIM algorithm based on a vector autoregressive model. In: China Satellite Navigation Conference (CSNC) 2015 Proceedings: Volume II. Springer, Heidelberg, pp. 125–142 (2015)
5. Wang, E., Jia, C., Tong, G., et al.: Fault detection and isolation in GPS receiver autonomous integrity monitoring based on chaos particle swarm optimization-particle filter algorithm. Adv. Space Res. **61**(5), 1260–1272 (2018)
6. Yun, H., Yun, Y., Kee, C.: Carrier phase-based RAIM algorithm using a Gaussian sum filter. J. Navig. **64**(1), 75–90 (2011)
7. Hewitson, S., Wang, J.: GNSS receiver autonomous integrity monitoring (RAIM) performance analysis. GPS Solut. **10**(3), 155–170 (2006)
8. Leick, A., Rapoport, L., Tatarnikov, D.: GPS Satellite Surveying, pp. 257–354. Wiley, New Jersey (2015)
9. Kaplan, E.D., Hegarty, C.: Understanding GPS: Principles and Applications, 3rd edn, pp. 661–701. Artech House, Boston (2017)
10. Paziewski, J., Sieradzki, R., Baryla, R.: Signal characterization and assessment of code GNSS positioning with low-power consumption smartphones. GPS Solut. **23**(4), 98 (2019)
11. Freda, P., Angrisano, A., Gaglione, S., et al.: Time-differenced carrier phases technique for precise GNSS velocity estimation. GPS Solut. **19**(2), 335–341 (2015)